Accepted for publication in:
SIAM Journal on Applied Mathematics
4th June 2018

WAVE PROPAGATION ALONG PERIODIC LAYERS*

CHRIS L. FARMER†, HILARY OCKENDON†, AND JOHN R. OCKENDON†

Abstract. Solutions for waves travelling transversely in a layered medium satisfy an exact recurrence relation when the transit time across each of the layers is the same. Using such solutions in an alternating-direction splitting method, high accuracy solutions can also be computed for wave propagation parallel to the layers. An asymptotic analysis uncovers the remarkable result that dispersion of waves parallel to the layers is very similar to the dispersion observed in the transverse case. This result is confirmed by the numerical solutions. The results are in general agreement with similar observations reported in the literature using different numerical and analytical methods.

Key words. wave propagation, periodic media, multiple scales, homogenization, dispersion

AMS subject classifications. 35B27, 34E13, 35L53, 35P25

1. Introduction.

Many authors have studied scalar wave propagation in layered media, both theoretically and numerically. The simplest configuration is the propagation of one-dimensional waves perpendicular to a periodic layered medium and for this case it has been shown that, over distances large compared to the layer thickness, the dominant signal propagates dispersively at a 'homogenised' wave speed which is slower than the speed of the leading disturbance. However, the wave reflections in a layered medium are more difficult to analyse when the signals are transmitted parallel to the layers and this is the problem that we address in this paper.

The results of [8] suggest that, in a layered medium in which the wave speed varies periodically from layer to layer, a source emits a signal which travels with a homogenised wave speed that is usually anisotropic. However in this paper we will mainly consider waves governed by the simple dimensionless scalar wave equation

$$\frac{\partial^2\phi}{\partial X^2}+\frac{\partial^2\phi}{\partial Y^2}=\frac{1}{c^2(Y)}\frac{\partial^2\phi}{\partial T^2}, \tag{1}$$

where c is piecewise constant and periodic in Y with period 2. Even though the homogenised wave speed for (1) is isotropic, the detailed structure of the wave field generated by an impulse at $T = 0$ is remarkably complicated.

A naïve asymptotic argument suggests that, in order to consider the disturbance over distances large compared to the width of the layers, we should set

$$X=\frac{x}{\epsilon},\ Y=\frac{y}{\epsilon},\ T=\frac{t}{\epsilon}, \tag{2}$$

where ϵ is some small parameter. We then write $\phi \sim \phi_0 + \epsilon\phi_1 + ...$ where the ϕ_i depend on x, y, t and Y. Then, as in [7], we find that ϕ_0 and ϕ_1 are independent of Y and ϕ_2 satisfies

$$\frac{\partial^2\phi_2}{\partial Y^2}+\frac{\partial^2\phi_0}{\partial x^2}+\frac{\partial^2\phi_0}{\partial y^2}=\frac{1}{c^2(Y)}\frac{\partial^2\phi_0}{\partial t^2}. \tag{3}$$

Then we can avoid secular terms that grow as $|Y| \to \infty$ only if ϕ_0 satisfies the

*Submitted to the editors DATE.
†OCIAM, Mathematical Institute, University of Oxford, Oxford, OX2 6GG, United Kingdom (farmer@maths.ox.ac.uk, hilary.ockendon@maths.ox.ac.uk, ock@maths.ox.ac.uk).

isotropic homogenised equation

$$\frac{\partial^2\phi_0}{\partial x^2}+\frac{\partial^2\phi_0}{\partial y^2}=\frac{1}{c_H^2}\frac{\partial^2\phi_0}{\partial t^2}, \tag{4}$$

where

$$\frac{1}{c_H^2}=\overline{\left(\frac{1}{c^2}\right)}, \tag{5}$$

and the overbar denotes averaging over a period 2 in Y.

For definiteness we now consider the solution in $x\cos\theta+y\sin\theta>0$ when the given boundary data is $\phi=1$ on $x\cos\theta+y\sin\theta=0$ for $t>0$ and the Cauchy data is $\phi=\dfrac{\partial\phi}{\partial t}=0$ at $t=0$. The case $\theta=\dfrac{\pi}{2}$ was considered in [7] and in this paper we will mainly consider $\theta=0$, but, in general, the solution can be rewritten in terms of the variables $z=x\cos\theta+y\sin\theta$, t and Y and then the homogenisation process leads to

$$\frac{\partial^2\phi_0}{\partial z^2}=\frac{1}{c_H^2}\frac{\partial^2\phi_0}{\partial t^2}. \tag{6}$$

We can continue the formal multiple scale asymptotic analysis for larger times exactly as in section 2 of [7]. In order to study the solution near the wavefront, we write $\xi=z-c_Ht$ and regard ϕ as a function[1] of ξ, Y and $\bar{t}=\epsilon^2t$, which are all $O(1)$. Then we can follow the earlier analysis to find that, if $\phi\sim\phi_0+\epsilon\phi_1+\epsilon^2\phi_2+...$, then ϕ_0 will satisfy

$$A\frac{\partial^4\phi_0}{\partial\xi^4}=\frac{\partial^2\phi_0}{\partial\xi\partial\bar{t}} \tag{7}$$

exactly as in (2.18) in [7] where $A=\dfrac{c_H}{4}\displaystyle\int_{-1}^{1}\left(\frac{c_H^2}{c(Y)^2}-1+4\sin^2\theta\right)\left(F(Y)-\bar{F}\right)dY$ with $F(Y)=\displaystyle\int_{-1}^{Y}\int_{-1}^{Y'}\left(\frac{c_H^2}{c(\tilde{Y})^2}-1\right)d\tilde{Y}\,dY'$. Hence we can see immediately that the term involving θ vanishes identically. When

$$c(Y)=\begin{cases}c_1, & -1<Y<0\\ c_2, & \quad 0<Y<1\end{cases}\quad, \tag{8}$$

we find that

$$A=\frac{c_H}{24}\left(\frac{c_H^2}{c_1^2}-1\right)\left(\frac{c_H^2}{c_2^2}-1\right), \tag{9}$$

where $\dfrac{2}{c_H^2}=\dfrac{1}{c_1^2}+\dfrac{1}{c_2^2}$.

The validity of (7) and (9) for all θ between 0 and $\pi/2$ is interesting and this isotropy is in accordance with some of the results illustrated in Figure 2 of [8]. However, in section 4, we will see that the detailed wave interactions that occur when

[1] Since ϵ is an arbitrary small parameter, instead of going to even longer times by scaling T with $1/\epsilon^3$, we could equally well have 'focussed' in on the narrow region where $x-c_Ht=O(\epsilon^{1/3})$ while keeping x,t of $O(1)$.

$\theta = \pi/2$ differ appreciably from those when $\theta = 0$. It can also be shown that the dispersion relation for (7, 9) is a special case of the dispersion relation (34) of [8], which was obtained by a systematic homogenisation in powers of the length-scale ratio.

The results of [8] also apply to the more general model

$$\frac{\partial}{\partial X}\left(\mu(Y)\frac{\partial \phi}{\partial X}\right) + \frac{\partial}{\partial Y}\left(\mu(Y)\frac{\partial \phi}{\partial Y}\right) = \rho(Y)\frac{\partial^2 \phi}{\partial T^2} \tag{10}$$

which, with a change of notation, is (1) of [8] for waves in a shear-free elastic medium. The same equation also describes Love waves in antiplane strain, when ϕ is the elastic displacement, μ is the shear modulus and ρ is the density. We now apply the same homogenisation procedure as before to (10). Assuming that μ and ρ have the same periodicity as c, our homogenisation procedure gives

$$\phi_0 = \phi_0(x, y, t) \tag{11}$$

and

$$\phi_1 = M(Y)\frac{\partial \phi_0}{\partial y}, \tag{12}$$

where

$$M(Y) = \int_0^Y \left(\frac{\mu_H}{\mu} - 1\right) dY \text{ where } \frac{1}{\mu_H} = \overline{\left(\frac{1}{\mu}\right)}. \tag{13}$$

This leads to the equation

$$\frac{\partial}{\partial Y}\left(\mu\frac{\partial \phi_2}{\partial Y}\right) + \left[\frac{d(\mu M)}{dY} + \mu_H\right]\frac{\partial^2 \phi_0}{\partial y^2} + \mu\frac{\partial^2 \phi_0}{\partial x^2} = \rho\frac{\partial^2 \phi_0}{\partial t^2} \tag{14}$$

and the condition that the solution for ϕ_2 should have no secular term as $Y \to \infty$ yields the anisotropic homogenised equation

$$\mu_H\frac{\partial^2 \phi_0}{\partial y^2} + \overline{\mu}\frac{\partial^2 \phi_0}{\partial x^2} = \overline{\rho}\frac{\partial^2 \phi_0}{\partial t^2}. \tag{15}$$

Note that this equation reduces to (4) when μ is constant.

When we continue the multiple scale analysis as above we now need to generalise the definition of ξ to

$$\xi = x\cos\theta + y\sin\theta - c_H t \tag{16}$$

where c_H is here given by

$$c_H^2 = \frac{\overline{\mu}}{\overline{\rho}}\cos^2\theta + \frac{\mu_H}{\overline{\rho}}\sin^2\theta \tag{17}$$

which is in accordance with Figure 4 of [8]. Finally we find that (7) still holds, but that the coefficient A now depends linearly on $\cos 2\theta$ and $\cos 4\theta$ with coefficients that are complicated integrals of μ and ρ. Henceforth we will only consider (1).

In [7] we were able to exploit the fact that when the wave speeds c_1 and c_2 are such that waves take equal times to traverse each layer, as in a Goupillaud medium [4], an exact discretisation was possible so that we had complete confidence in the numerical predictions. Based on this experience with one-dimensional transverse wave propagation, we begin in section 2 by proposing an algorithm to shed light on the mathematical properties of waves propagating parallel to the layers in alternating-direction Goupillaud media, for which an exact discretisation is no longer possible. This algorithm allows us to compute high-resolution numerical solutions on relatively coarse spatial grids. The results are of sufficient quality to corroborate detailed asymptotic calculations.

Next, in section 3, we will address the problem of a 'leaky' waveguide where the wave speed c is constant and homogeneous Dirichlet boundary conditions are applied. Our principal reason for devoting a section to this problem is the fact that it gives us many clues about the waves generated when solving the bilayer problem, where we will find that the wave in the fast layer will leak energy into the slow layer and create a disturbance travelling at an intermediate speed c_H.

Sections 2 and 3 are precursors to the principal results of the paper in section 4, where we consider wave propagation in periodic bilayers.

2. An alternating-direction Goupillaud medium. Our strategy for constructing approximate numerical solutions for the wave equation will use operator splitting, in particular the method of dimensional splitting. This uses solutions of one-dimensional wave equations in each direction, and weaves them into a two-dimensional solution. Recalling that a Goupillaud medium is a layered medium in which waves take the same time to cross each layer, we first show how a Goupillaud medium leads to an exact discretisation of the one-dimensional wave equation. Then a general method of constructing an 'alternating-direction Goupillaud medium' will be proposed and we close this section with a description of the dimensional splitting algorithm used in our subsequent numerical experiments.

Note that in this section, superscripts x and y are used to denote directions.

2.1. Wave equations in conservation form. Consider the system of conservation laws

$$\frac{\partial q}{\partial T} + A\frac{\partial q}{\partial X} + B\frac{\partial q}{\partial Y} = 0, \tag{18}$$

where

$$A = \begin{bmatrix} 0 & c^2 & 0 \\ 1 & 0 & 0 \\ 0 & 0 & 0 \end{bmatrix}, \tag{19}$$

$$B = \begin{bmatrix} 0 & 0 & c^2 \\ 0 & 0 & 0 \\ 1 & 0 & 0 \end{bmatrix}, \tag{20}$$

and

$$q = \begin{bmatrix} \phi \\ u \\ v \end{bmatrix} \tag{21}$$

so that ϕ satisfies (1)[2]. Also suppose that $q = 0$ at $T = 0$, $X > 0$ and ϕ is prescribed at $X = 0$, $T > 0$.

[2]Our alternating-direction Goupillaud algorithm generalises in the obvious way to the model (10).

2.2. One-dimensional Goupillaud media. When $q = q(Y, T)$, we let τ be a positive time interval called the 'time step', and let $Y_j, j = 0, 1, ..., n^y$ be a sequence of $n^y + 1$ mesh points with $Y_0 = 0$, $Y_j - Y_{j-1} = h_j > 0$ for $j > 0$ and $Y_{n^y} = L^y$. From now on we assume that c is piecewise constant such that $c(Y) = c_j$ for $Y \in (Y_{j-1}, Y_j)$ with,

$$c_j \tau = h_j. \tag{22}$$

In a Goupillaud medium with piecewise-constant initial data which is constant on the cells (Y_{j-1}, Y_j) and in which any time dependence in the boundary data is also piecewise constant with discontinuities at the times $T_n = n\tau$ for $n = 0, 1, ...$, it is possible to discretise the equations exactly [6],[7]. The solutions have a particularly simple form at each time T_n when they evolve to a new spatially piecewise-constant state and this exact property is also enjoyed by the Godunov method for solving first-order linear hyperbolic systems when the Courant number is unity. However we stress that the piecewise solutions in one dimension are exact. We note that in numerical experiments a boundary condition is needed at $Y = L^y$. By choosing L^y to be sufficiently large that, for the chosen final time of the experiment, no wave has reached the far boundary, any reasonable boundary condition will suffice and, for definiteness, we set $\phi = 0$ at $Y = L^y$.

We also note that, if the Goupillaud medium is refined by dividing each cell into r equal segments and the time step τ is also divided into r equal time steps of duration τ/r, then the refined system also has the Goupillaud property.

2.3. An alternating-direction Goupillaud medium in two dimensions. In two dimensions it is no longer possible to build a Goupillaud medium with piecewise constant wave speeds such that the Goupillaud property holds in any direction. It is, however, possible to build a medium with an alternating-direction Goupillaud property if we choose the time steps in each direction appropriately. In fact it is possible, with little extra complication, to consider an alternating-direction Goupillaud medium whose geometry is more general than just periodic layers. The scheme for this general case is as follows.

Consider a two-dimensional rectangular strip $(0, L^x) \times (0, L^y)$ for strictly positive L^x and L^y. Introduce two sequences of points $0 = X_0 < X_1 < ... < X_i < .... < X_{n^x} = L^x$ and $0 = Y_0 < Y_1 < ... < Y_j < .... < Y_{n^y} = L^y$. These points characterise a rectangular grid of cells $\omega_{i,j} = (X_{i-1}, X_i) \times (Y_{j-1}, Y_j)$. Let $h^x_i = X_i - X_{i-1}$ and $h^y_j = Y_j - Y_{j-1}$.

In the following construction we take as given (i) L^y, (ii) the number of cells n^x and n^y in the x and y-directions, (iii) the wave speed, $c_{1,1}$ in the first cell and (iv) two sequences of strictly positive integers $m^x_j, j = 1...n^y$ and $m^y_i, i = 1...n^x$ such that these integers are less than $\min\{n^x, n^y\}$.

The values of h^x_i, h^y_j and the length L^x, are chosen to satisfy the geometrical conditions

$$\sum_{i=1}^{n^x} h^x_i = L^x \tag{23}$$

and

$$\sum_{j=1}^{n^y} h^y_j = L^y. \tag{24}$$

We also require the wave speeds $c_{i,j}$ in each of the cells $(i,j) \neq (1,1)$ and the time step τ to be such that

$$c_{i,j}\frac{\tau}{m_j^x} = h_i^x, \tag{25}$$

and

$$c_{i,j}\frac{\tau}{m_i^y} = h_j^y. \tag{26}$$

These are the Goupillaud conditions along each i-strip or j-strip when considered as a one-dimensional medium.

It follows from (25) and (26) that,

$$h_j^y = \frac{h_i^x m_j^x}{m_i^y}, \tag{27}$$

and then, using (24), that h_i^x/m_i^y is a constant independent of i. Thus

$$\frac{h_i^x}{m_i^y} = \lambda = \frac{L^y}{\sum_{j=1}^{n^y} m_j^x}, \tag{28}$$

where λ is a constant.

It then follows that $\tau = \dfrac{h_1^y m_1^y}{c_{1,1}}$, $h_i^x = \lambda m_i^y$, $h_j^y = \lambda m_j^x$, and $c_{i,j} = \dfrac{h_j^y m_i^y}{\tau}$. The length L^x is found from (23). The quantities τ/m_j^x and τ/m_i^y can than be used as local time steps in each row or column of the alternating-direction Goupillaud medium, thus leading to a one-dimensional recurrence relation in each direction.

As in the one-dimensional case, a refinement can be made whereby the time step, τ can be divided into r intervals of τ/r and the cells can be divided into r^2 equal rectangles with sizes h_i^x/r and h_j^y/r. The wave speed in each of the cell divisions is set to the wave speed in the parent Goupillaud cell.

Now assume that (i) q_0 is a piecewise-constant initial condition, (ii) that c defines an alternating-direction Goupillaud medium and (iii) that at time $T_n = n\tau$ an approximate solution q_n has been found. To find an approximate solution q_{n+1} at time $T_{n+1} = (n+1)\tau$, we solve the following four equations:

$$\left(\frac{\partial}{\partial T} + A\frac{\partial}{\partial X}\right)q^{xx} = 0, \text{ with } q^{xx}(X,Y,T_n) = q_n, \tag{29}$$

$$\left(\frac{\partial}{\partial T} + B\frac{\partial}{\partial Y}\right)q^{xy} = 0, \text{ with } q^{xy}(X,Y,T_n) = q^{xx}(X,Y,T_{n+1}), \tag{30}$$

$$\left(\frac{\partial}{\partial T} + B\frac{\partial}{\partial Y}\right)q^{yy} = 0, \text{ with } q^{yy}(X,Y,T_n) = q_n, \text{ and} \tag{31}$$

$$\left(\frac{\partial}{\partial T} + A\frac{\partial}{\partial X}\right)q^{yx} = 0, \text{ with } q^{yx}(X,Y,T_n) = q^{yy}(X,Y,T_{n+1}). \tag{32}$$

Each of these one-dimensional problems can be solved exactly by virtue of the Goupillaud property, where the appropriate local time step is used over the appropriate number of time steps according to the direction and the row or column in which we are solving the equation. In each special problem it is necessary to impose particular boundary conditions. This is done using formulae derived from the associated Riemann problems as described, for example, in [6].

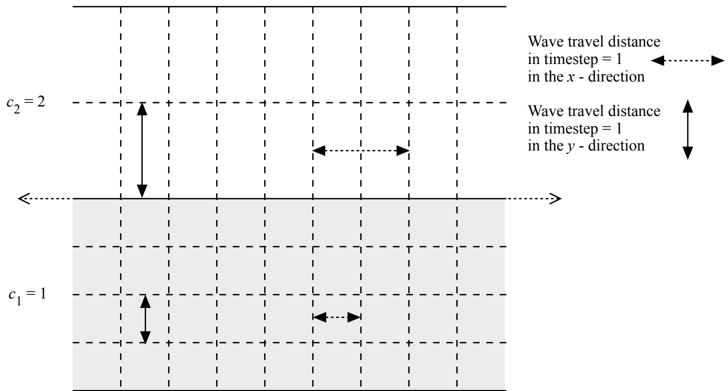

FIG. 1. *An alternating-direction Goupillaud grid where $c_1 = 1$, $c_2 = 2$. The shaded region indicates $c_1 = 1$. In rows of cells where $c_2 = 2$ the time step is split so that two time steps are performed for each x-direction solution.*

The approximate solution q_{n+1} at time T_{n+1} is finally found from the equation,

$$q_{n+1} = \frac{1}{2}\big[q^{xy}(X, Y, T_{n+1}) + q^{yx}(X, Y, T_{n+1})\big]. \tag{33}$$

This formula, as far as we know, was first given as equation (25) in [10]. In the next two sections we will apply this algorithm to wave propagation along layers[3].

Figure 1 shows an example of an alternating-direction Goupillaud grid, where $c_1 = 1$, $c_2 = 2$, $n^y = 6$ with $m^x_j = 1$ for $j = 1 : 4$ and $m^x_j = 2$ for $j = 5 : 6$ and $m^y_i = 1$ for all i.

3. Wave propagation along a single layer. As a preliminary to our main objective of understanding waves in bilayers we now consider (1) when c is constant, subject to the 'leaky' boundary conditions

$$\phi = 0 \text{ on } Y = 0, 2 \tag{34}$$

and

$$\phi = H(T) \text{ on } X = 0; \tag{35}$$

here $H(T)$ is the Heaviside function, and

$$\phi = \frac{\partial \phi}{\partial T} = 0 \text{ at } T = 0, X > 0. \tag{36}$$

Henceforth in this section we take $Y \in (0, 2)$. We first present some numerical results, then the analytical solution for small times and finally some asymptotic results for large times. In section 4 we will follow the same plan for the bilayer problem.

[3]This particular splitting method does not seem to have been widely used, if at all. In preliminary numerical experiments using more common schemes which require less storage than (33), instability occurred in the corners of the domain where there is a singularity in the boundary conditions. By using (33) we found that such instabilities were absent and the agreement with analytical early-time solutions was satisfactory.

3.1. Numerical predictions. In the special case that $c = 1$ throughout a rectangular domain, an alternating-direction Goupillaud medium results by setting $m^x_j = 1$ and $m^y_i = 1$ in all cells, which are then square with sides h such that $h^y_j = h = 1/n^y$ and $h^x_i = h$. The time step is then $\tau = h$ in all of the rows and columns of the grid. Figures 2 and 3 show the numerical solution after the wave has propagated a distance $1/2$ and 50 in the X-direction. In this simulation $n^y = 50$. The figures have a different scale in each direction, and show one half of the domain, the solution being symmetric about $Y = 1$.

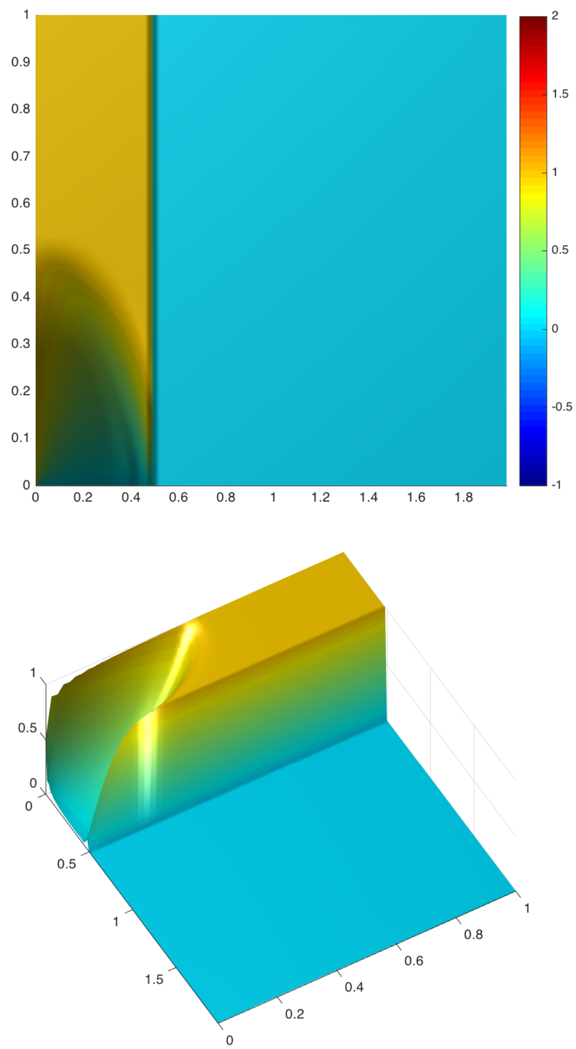

FIG. 2. *Plan and perspective views of ϕ at $T = 0.5$.*

3.2. Exact solution for $T < 1/c$. Initially a step function $\phi = H(T - X/c)$ propagates from $X = 0$ and the effect of the boundaries at $Y = 0, 2$ is only felt near the corners $(0, 0)$ and $(0, 2)$. Near $(0, 0)$ we can find a similarity solution by writing

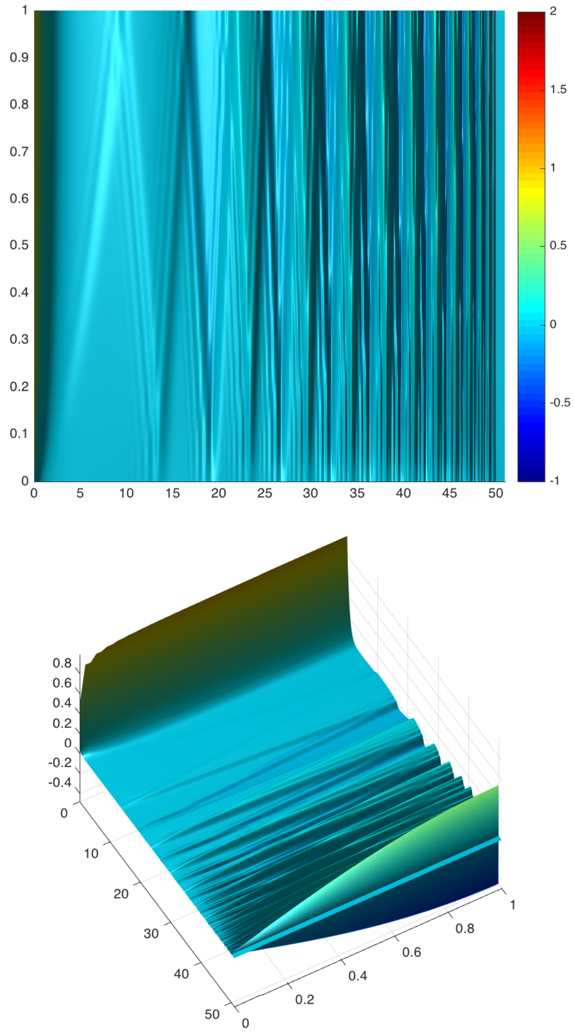

FIG. 3. *Plan and perspective views of ϕ at $T = 50$.*

$r = X/T$ and $s = Y/T$ so that (1) becomes

$$(r^2 - c^2)\frac{\partial^2\phi}{\partial r^2} + 2rs\frac{\partial^2\phi}{\partial r\partial s} + (s^2 - c^2)\frac{\partial^2\phi}{\partial s^2} + 2r\frac{\partial\phi}{\partial r} + 2s\frac{\partial\phi}{\partial s} = 0. \tag{37}$$

This equation is hyperbolic or elliptic depending whether $r^2 + s^2$ is greater or less than c^2 respectively, and the structure of the solution is sketched in Figure 4. For $T < 1/c$ there are two elliptic regions A and C on either side of a hyperbolic region B which is bounded by $r = 0$, c and the two quarter circles. In the hyperbolic region the characteristics are the tangents to these circles and hence the solution in B is just $\phi = 1$. In region A we need to solve (37) subject to the boundary conditions

$$\phi = 0 \text{ on } s = 0; \phi = 1 \text{ on } r = 0 \text{ and } r^2 + s^2 = c^2. \tag{38}$$

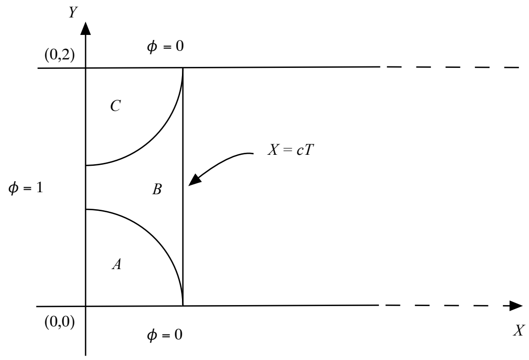

FIG. 4. *The early time analytical solution for the wave guide problem.*

This is similar to a problem solved in, for example, [5] and we can transform (37) into Laplace's equation by writing

$$\tan\theta = \frac{s}{r}, \text{ and } \cosh\beta = c(r^2+s^2)^{-1/2}, \tag{39}$$

so that (37) and (38) become

$$\frac{\partial^2\phi}{\partial\beta^2} + \frac{\partial^2\phi}{\partial\theta^2} = 0, \tag{40}$$

with $\phi = 0$ on $\theta = 0$ ($\beta > 0$), $\phi = 1$ on $\theta = \pi/2$ ($\beta > 0$), and $\phi = 1$ on $\beta = 0$ ($0 < \theta < \pi/2$). By conformally mapping this semi-infinite strip onto the half-plane, we find that

$$\phi = \frac{1}{\pi}\cos^{-1}\left[\frac{c^2(r^2-s^2) - r^2(r^2+s^2)}{c^2(r^2+s^2) - r^2(r^2+s^2)}\right], \tag{41}$$

which is in good agreement with the numerical solution shown in Figure 2. However, when $T = 1/c$, the two quarter circles in Figure 4 meet and thereafter the similarity solution is no longer available. Nonetheless, we note that the wave fronts from the corners can only travel with speed c, so that for all time there will be a region where $\phi = 1$ bounded by the front $X = cT$ and two circles of radius cT centred on $(0, 0)$ and $(0, 2)$.

3.3. Long time asymptotics. Although the similarity solution (41) is only valid for $T < 1/c$, an exact solution can always be written down using transform methods. We take a complex Laplace transform in T and a Fourier sine transform in X to reduce the problem to an ordinary differential equation in Y. We define

$$\tilde{\phi} = \int_0^\infty \int_0^\infty \phi e^{i\omega T} \sin kX\,dX\,dT, \tag{42}$$

with $\Im\omega > 0$ and k real, and then (1), (35) and (36) lead to

$$\frac{d^2\tilde{\phi}}{dY^2} + \lambda^2\tilde{\phi} = -\frac{ik}{\omega}, \tag{43}$$

where $\lambda^2 = \frac{\omega^2}{c^2} - k^2$ and, from (34), $\tilde{\phi} = 0$ on $Y = 0, 2$. Hence

$$\tilde{\phi} = \frac{-ik}{\omega(\omega^2/c^2 - k^2)}(1 - \cos\lambda Y - \csc 2\lambda(1 - \cos 2\lambda)\sin\lambda Y). \tag{44}$$

The inversion formula for ϕ is

$$\phi = \frac{1}{\pi^2}\int_0^\infty \sin kX \int_\Gamma e^{-i\omega T}\tilde{\phi}\,d\omega dk, \tag{45}$$

where Γ is a Bromwich contour on which $\Im\omega > 0$. Since $\tilde{\phi}$ is an even function of λ, it has no branch points as a function of ω and we can invert the Laplace transform by closing the contour in the lower half of the ω-plane and calculating the residues of $\tilde{\phi}e^{-i\omega T}$ at its poles which occur where $\omega = 0$ and $\omega = \pm c\sqrt{(k^2 + \frac{n^2\pi^2}{4})}$, where n is an odd integer. At $\omega = 0$, $\lambda^2 = -k^2$ the residue is

$$R_0(k, Y) = \frac{i}{k}[1 - \cosh kY - \frac{(1 - \cosh 2k)}{\sinh 2k}\sinh kY], \tag{46}$$

and at $\omega = \pm c\sqrt{(k^2 + \frac{n^2\pi^2}{4})}$, $\lambda^2 = \frac{(n\pi)^2}{4}$, the combined residue is

$$R_n(k, Y, T) = -\frac{4ik\sin\frac{n\pi Y}{2}\cos c\sqrt{k^2 + \frac{n^2\pi^2}{4}}T}{n\pi(k^2 + \frac{n^2\pi^2}{4})}. \tag{47}$$

Hence, from (45),

$$\phi = -\frac{2i}{\pi}\int_0^\infty \Big(R_0(k, Y) + \sum_{\substack{n \text{ odd} \\ n>0}} R_n(k, Y, T)\Big)\sin kX\,dk, \tag{48}$$

the convergence of the integral being non-uniform as $X \to 0$. The first term in (48) is the steady solution of the problem which is the 'harmonic footprint' which remains for finite X as $T \to \infty$ and it can be shown that this integrates to

$$\phi_0 = \frac{4}{\pi}\sum_{\substack{n \text{ odd} \\ n>0}} \frac{1}{n}\sin\frac{n\pi Y}{2}e^{-\frac{n\pi}{2}X}. \tag{49}$$

In order to study the large-time asymptotics in the other terms in (48), we write $\phi = \phi_0 + \sum_{\substack{n \text{ odd} \\ n>0}} \phi_n \sin\frac{n\pi Y}{2}$ and note that

$$\begin{aligned}\frac{\partial\phi_n}{\partial T} &= -\frac{8c}{n\pi^2}\frac{\partial}{\partial X}\left\{\int_0^\infty \frac{\sin c\sqrt{k^2 + \frac{n^2\pi^2}{4}}T\cos kX}{\sqrt{k^2 + \frac{n^2\pi^2}{4}}}dk\right\} \\ &= \begin{cases} -\frac{4c}{n\pi}\frac{\partial}{\partial X}J_0(\frac{n\pi}{2}\sqrt{c^2T^2 - X^2}), & 0 < X < cT \\ 0, & cT < X \end{cases}\end{aligned} \tag{50}$$

as shown in [2], where J_0 is the Bessel function. Hence using (36), for $0 < X < cT$,

$$\phi = 1 - 2X\sum_{\substack{n \text{ odd} \\ n>0}} \left\{\int_X^{cT} \frac{J_1(\frac{n\pi}{2}\sqrt{\tau^2 - X^2})}{\sqrt{\tau^2 - X^2}}d\tau\right\}\sin\frac{n\pi Y}{2}. \tag{51}$$

We note that for an energy-conserving waveguide, in which (34) is replaced by $\partial\phi/\partial Y = 0$ on $Y = 0, 2$, the solution is $\phi = H(cT - X)$ which corresponds to the first term in (51). However for the leaky waveguide, even the large-time asymptotic behaviour is not easy to discern. From (51) we see that we need to consider the integrals

$$I_n = \int_X^{cT} \frac{J_1(\frac{n\pi}{2}\sqrt{\tau^2 - X^2})}{\sqrt{\tau^2 - X^2}} d\tau = \int_0^{\sqrt{c^2T^2 - X^2}} \frac{J_1(\frac{n\pi}{2}\eta)}{\sqrt{X^2 + \eta^2}} d\eta, \tag{52}$$

where $\eta = \sqrt{(\tau^2 - X^2)}$. We will see that there are three different regimes when T is large, depending on the magnitude of X/T.

(i) When $X/T \ll 1$, we can approximate I_n by

$$I_n \sim \int_0^{\infty} \frac{J_1(\frac{n\pi}{2}\eta)}{\sqrt{X^2 + \eta^2}} d\eta = \frac{1 - e^{-\frac{n\pi}{2}X}}{\frac{n\pi}{2}X} \tag{53}$$

using [3] and, using (51), we retrieve the steady solution (49).

(ii) When X/T is $O(1)$ but not close to c, writing $\eta = X\tilde{\eta}$ in (52) gives

$$I_n = \int_0^{\sqrt{\frac{T^2c^2}{X^2} - 1}} \frac{J_1(\frac{n\pi}{2}X\tilde{\eta})}{\sqrt{1 + \tilde{\eta}^2}} d\tilde{\eta} \tag{54}$$

and, ignoring a small contribution from the region $\tilde{\eta} = O(1/nX)$, we can use the asymptotic representation of J_1 to write

$$I_n \sim \sqrt{\frac{4}{n\pi X}} \Re\left[e^{-3i\pi/4} \int_0^{\sqrt{\frac{c^2T^2}{X^2} - 1}} \frac{e^{i\frac{n\pi}{2}X\tilde{\eta}}}{\sqrt{\tilde{\eta}(1 + \tilde{\eta}^2)}} d\tilde{\eta} \right], \tag{55}$$

which, as $X \to \infty$, tends to

$$\sqrt{\frac{4}{n\pi X}} \Re\left[e^{-3i\pi/4} \left(\frac{e^{i\frac{n\pi}{2}\sqrt{c^2T^2 - X^2}}}{(c^2T^2 - X^2)^{1/4}} + O(T^{-1}) \right) \right]. \tag{56}$$

When the Y-dependence is reinstated using (51), terms such as (56) correspond to combinations of plane waves travelling obliquely across the layer as can be seen in Figure 3.

(iii) The final regime is close to the wave front where $\zeta = X - cT = O(1)$ and so $c^2T^2/X^2 - 1 \sim -2\zeta/X$. Then we can approximate I_n by

$$\int_0^{\sqrt{\frac{-2\zeta}{X}}} J_1\Big(\frac{n\pi}{2}X\tilde{\eta}\Big) d\tilde{\eta} = \frac{2}{n\pi X}\bigg(1 - J_0\Big(\frac{n\pi}{2}\sqrt{-2\zeta X}\Big)\bigg). \tag{57}$$

As expected $I_n = 0$ when $\zeta = 0$, but this expression exhibits rapid oscillatory decay to $1/n\pi X$ as ζ decreases, eventually matching with (56) as $\zeta \to -\infty$. These three regimes can be seen clearly in Figure 3. We note that the major contribution to I_n as $T \to \infty$ will come from values of ζ which are between zero and the first zero of $J_0(\frac{n\pi}{2}\sqrt{-2\zeta/X})$. The fact that the integral of I_n over this short region is of $O(1/n^2)$ as $n \to \infty$ reveals that the local average of ϕ near $X = cT$ has a roughly parabolic shape, thus explaining the profile seen near $X = cT$ in the numerical solution in Figure 3. We will now see that wave propagation in a bilayer leads to a similar 3-regime asymptotic structure.

4. Wave propagation along periodic bilayers. In this section we consider the solution of (1) in a periodic medium where, for analytical convenience, we now set

$$c(Y) = \begin{cases} c_1, & -1 < Y < 0 \\ c_2, & 0 < Y < 1 \end{cases}, \tag{58}$$

where $c_2 > c_1$. We take ϕ and $\frac{\partial \phi}{\partial Y}$ to be continuous at $Y = 0$, but we note that if we were solving (10) and $\mu(Y)$ was not constant, we would need instead to take $\mu \frac{\partial \phi}{\partial Y}$ to be continuous at $Y = 0$. We also take as boundary and initial conditions

$$\begin{gathered} \phi = H(T) \text{ on } X = 0, \\ \phi = \frac{\partial \phi}{\partial T} = 0 \text{ at } T = 0, X > 0. \end{gathered} \tag{59}$$

To exploit the symmetry of the problem we use homogeneous Neumann conditions at the midpoints of the layers and solve the problem in $-1/2 < Y < 1/2$ with

$$\frac{\partial \phi}{\partial Y} = 0 \text{ at } Y = \pm\frac{1}{2}, \tag{60}$$

which is equivalent to imposing periodic boundary conditions.

4.1. Numerical predictions. We consider the case where $c_1 = 1$ and $c_2 = 2$. For the numerical simulations, an alternating-direction Goupillaud medium results by setting $n^y = 300$ with $m_j^x = 1$ for $j = 1 : 200$ and $m_j^x = 2$ for $j = 201 : 300$ and $m_i^y = 1$ for all i. The cell dimensions are then such that $h_j^y = 1/400$ for $j = 1 : 200$, $h_j^y = 1/200$ for $j = 201 : 300$ and $h_i^x = 1/400$. The overall time step is then $\tau = 1/400$ in both layers, but is split into two equal sub-steps in the fast layer when solving the x-direction equations. Figures 5 and 6 show the numerical solution at $T = 0.24$ and $T = 50$; note that the figures, which show one half of each layer, are scaled differently in the X and Y directions. Figure 7 shows ϕ at $T = 50$ along the lines $Y = -0.5$ and $Y = 0.5$.

4.2. Small time analysis, $T = O(1)$. Because of the wave transmission and reflection between the layers, we cannot find an explicit small time solution as was possible in section 3.2. However we can still formulate the problem as a similarity solution in terms of $r = X/T$ and $s = Y/T$ which will be valid for $c_2 T < 1/2$. In this case we need to solve (37) with c replaced by c_1 in $s < 0$ and by c_2 in $s > 0$. Once again the equation near $X = Y = 0$ will be hyperbolic or elliptic according as $r^2 + s^2$ is greater or less than c_i^2 and, as shown in Figure 8, ϕ will be unity in the shaded regions. There is now an additional region APC where (37) is hyperbolic but in which ϕ is neither 0 nor 1. This region is bounded by (i) the Mach line AP which makes an angle $\gamma = \sin^{-1} c_1/c_2$ with the interface, (ii) the elliptic/hyperbolic boundary on CP and (iii) the interface between the layers AC. There will also be a jump of magnitude 1 along the line BC. In this region we can rewrite (37) in terms of the characteristic variables

$$\theta = \tan^{-1} \frac{s}{r}, \quad \alpha = \sin^{-1} \frac{c_1}{\sqrt{r^2 + s^2}} \tag{61}$$

so that, when $r^2 + s^2 > c_1^2$, (37) becomes

$$\frac{\partial^2 \phi}{\partial \theta^2} - \frac{\partial^2 \phi}{\partial \alpha^2} = 0. \tag{62}$$

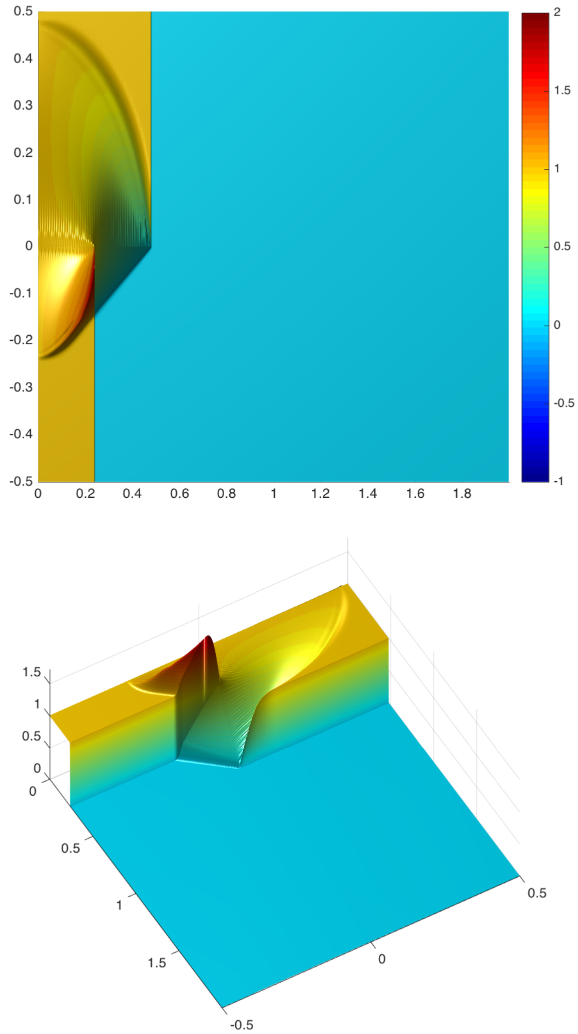

FIG. 5. *Plan and perspective views of ϕ at $T = 0.24$ and where $c_1 = 1$, $c_2 = 2$.*

In the elliptic regions E_i, the appropriate canonical variables are θ and

$$\beta_i = \cosh^{-1}\left(\frac{c_i}{\sqrt{r^2+s^2}}\right), \tag{63}$$

where $i = 1, 2$ and then (37) becomes Laplace's equation in both regions. Although it is still possible to map the regions E_1 and E_2 into the upper and lower half-plane with conditions given on the real axis, it is no longer possible to solve the problem analytically. However the numerical solution shown in Figure 5 for $T = 0.24$ conforms to the structure described in Figure 8 and helps us to understand how the solution will evolve for larger times.

In the light of the above discussion, we can anticipate certain general features of the solution over longer times. First, we expect the leading wave fronts to be as shown in Figure 9; there will be jumps of unity in ϕ across $X = c_2T$ in $0 < Y < 1$ and across

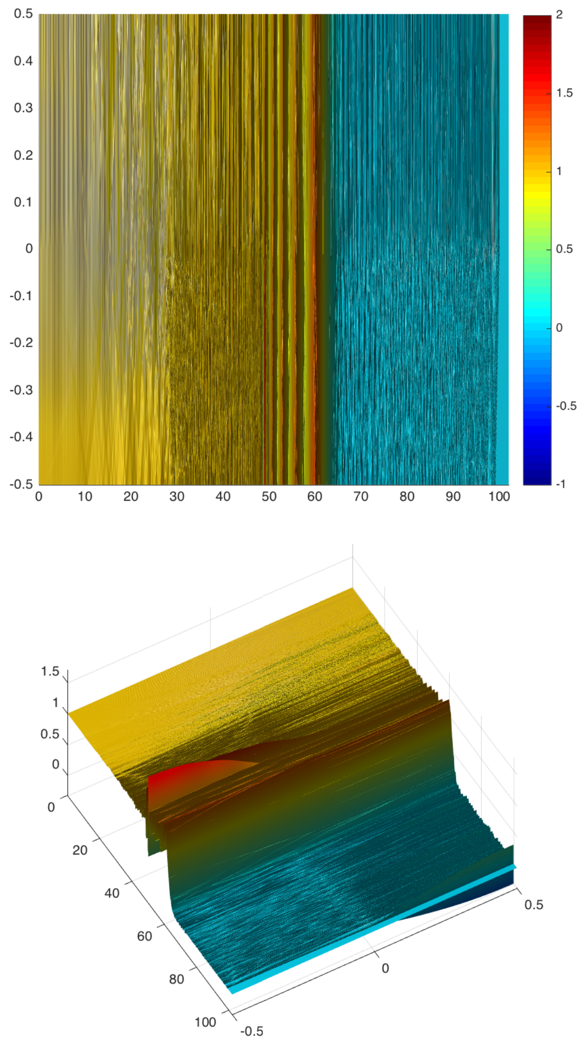

FIG. 6. *Plan and perspective views of ϕ when $T = 50$ and where $c_1 = 1$, $c_2 = 2$.*

$X = c_1T$ in $-1 < Y < 0$, but the numerical solutions suggest that ϕ will decay rapidly behind these fronts. However, we do not expect that the numerical scheme will be able to capture these very thin spikes at all accurately. Furthermore ϕ vanishes on the Mach lines DE and EF, which make an angle of γ with the X-axis, but ϕ will have a jump in its normal derivative on these lines. The homogenisation described in section 1 suggests that for times that are long compared to unity the main variations in ϕ will travel with speed c_H in both layers and this can be seen in the numerical solutions in Figures 6 and 7. However the field elsewhere will, as time increases, contain multiple reflections and transmissions at the interfaces between the layers and these are not well described by the homogenised solution even using the dispersive equation (7). We will now address the full problem using transform methods as in section 3 and show how the multiple reflections observed above are associated with the singularities

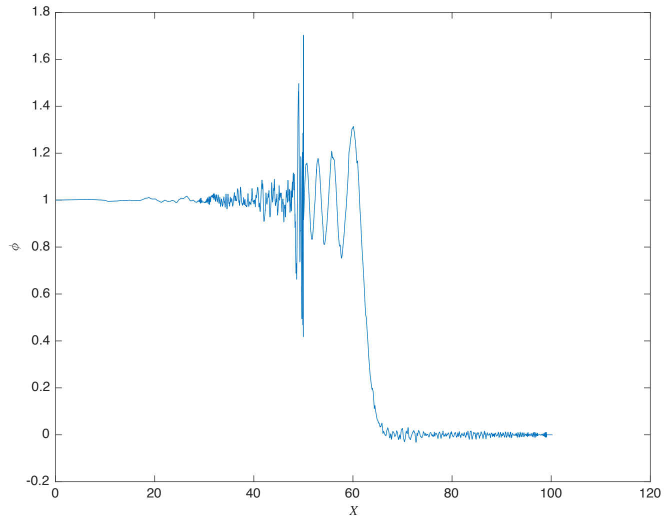

(a) $Y = -0.5$

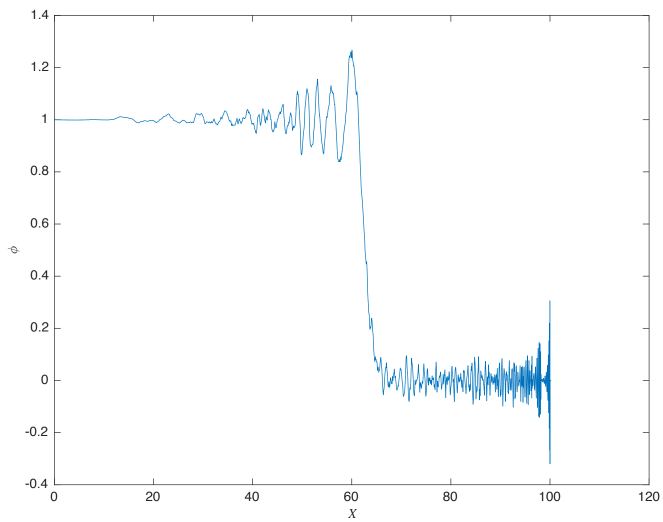

(b) $Y = 0.5$

FIG. 7. *Plot of ϕ against X when $T = 50$ with $c_1 = 1$, $c_2 = 2$.*

in the transform of the solution.

4.3. Transform analysis. Just as in section 3, we can employ the double transform (42) for real values of k and positive values of $\Im\omega$ to obtain a representation of the solution valid for all T. Using (59), we find that

$$\frac{d^2\tilde{\phi}}{dY^2} + {\lambda_i}^2\tilde{\phi} = -\frac{ik}{\omega}, \tag{64}$$

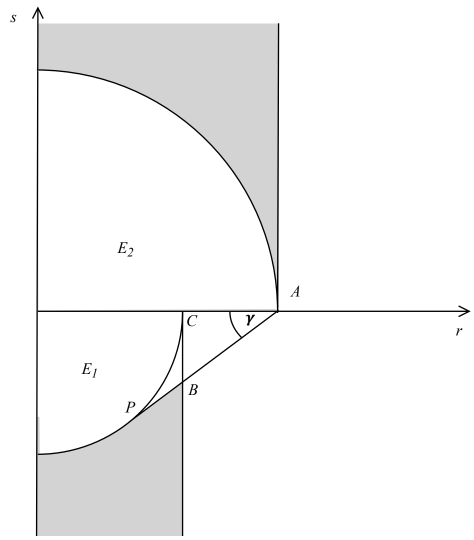

FIG. 8. *Analytical structure of the solution for the bilayer problem at small times.*

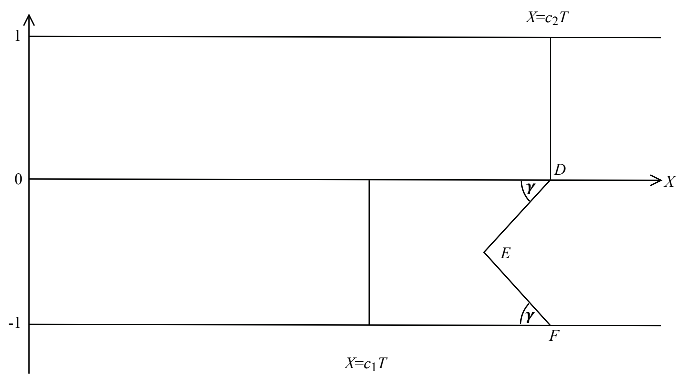

FIG. 9. *Schematic of the leading fronts in the bilayer problem.*

where

$$\lambda_1^2 = \frac{\omega^2}{c_1^2} - k^2, \quad -1/2 < Y < 0,$$
$$\lambda_2^2 = \frac{\omega^2}{c_2^2} - k^2, \qquad 0 < Y < 1/2, \tag{65}$$

and, for definiteness, we define $\lambda_i \sim \omega/c_i$ as $|\omega| \to \infty$. Hence

$$\tilde{\phi} = -\frac{ik}{\omega\lambda_1^2} + P\cos\lambda_1 Y + Q\sin\lambda_1 Y, \quad -1/2 < Y < 0,$$
$$\tilde{\phi} = -\frac{ik}{\omega\lambda_2^2} + R\cos\lambda_2 Y + S\sin\lambda_2 Y, \qquad 0 < Y < 1/2, \tag{66}$$

where P,Q,R and S are determined by imposing continuity of ϕ and $\frac{\partial\phi}{\partial Y}$ at $Y = 0$ and using conditions (60). These functions all depend on ω, λ_1^2 and λ_2^2 and are set out in the Appendix. In particular, we note that the only singularities of these functions are poles in the ω-plane at points where $\omega = 0$, $c_1 k$, $c_2 k$ or where

$$\Delta = \lambda_1 \tan \frac{\lambda_1}{2} + \lambda_2 \tan \frac{\lambda_2}{2} = 0. \tag{67}$$

As a check, in the homogeneous case when $c_1 = c_2 = c$, we find that

$$\tilde{\phi} = \frac{-ik}{\omega(\omega^2/c^2 - k^2)}, \tag{68}$$

and using (45) to invert this transform leads to

$$\phi = H(cT - X) \tag{69}$$

as expected. Also we note that, in this case, (67) is satisfied when

$$\omega^2 = c^2(k^2 + 4n^2\pi^2), \tag{70}$$

although $\tilde{\phi}$ only has poles when $n = 0$.

In general when c_1 and c_2 are distinct, the curves given by the dispersion relation (67) need to be plotted in the (k, ω) plane numerically in order to determine the position of the poles of $\tilde{\phi}$ in the complex ω-plane. Guided by (70), we label the branches by $\omega = \Omega_n$ $(n \geq 0)$ where

$$\Omega_n^2 \sim c_1^2 k^2 + (2n+1)^2 \pi^2 c_1^2 + \cdots \tag{71}$$

as $k \to \infty$. As shown in Figure 10, these branches all develop points of inflection. For large values of ω and k, the emergence of a so-called *pseudo-branch* close to the line $\omega = c_2 k$ can be discerned. This is similar to the dispersion relation described in [9] which includes both pseudo-branches and quasi-crossings. The detailed structure of the branches near $\omega = c_2 k$ for large ω, k can be revealed by writing

$$k = \frac{2n\pi}{S} + \kappa, \;\; \omega = \frac{2n\pi c_2}{S} + \Omega,$$

where $S = \sqrt{c_2^2/c_1^2 - 1}$, and noting that, with

$$\mu_1 = \frac{1}{2S}\left(\frac{c_2 \Omega}{c_1^2} - \kappa\right), \;\; \mu_2 = \sqrt{\frac{n\pi}{S}}\left(\frac{\Omega}{c_2} - \kappa\right)^{1/2},$$

where μ_1 and μ_2 are $O(1)$, (67) becomes

$$n\pi \tan \mu_1 + \mu_2 \tan \mu_2 = O\left(\frac{1}{n}\right) \tag{72}$$

as $n \to \infty$. This relation between μ_1 and μ_2 is plotted in Figure 11 for $n = 10$ where μ_2 is real. The lattice of 'quasi-crossings' that emerges when μ_2 is real corresponds to the parallelograms apparent in Figure 10 above the line $\omega = c_2 k$ for large k.

When we consider the inversion of (66), we see, from (45), that the solution in $-1/2 < Y < 0$ is

$$\phi = \frac{1}{\pi^2} \int_0^\infty \sin kX \int_\Gamma e^{-i\omega T} \left(\frac{-ik}{\omega \lambda_1^2} + P \cos \lambda_1 Y + Q \sin \lambda_1 Y\right) d\omega dk. \tag{73}$$

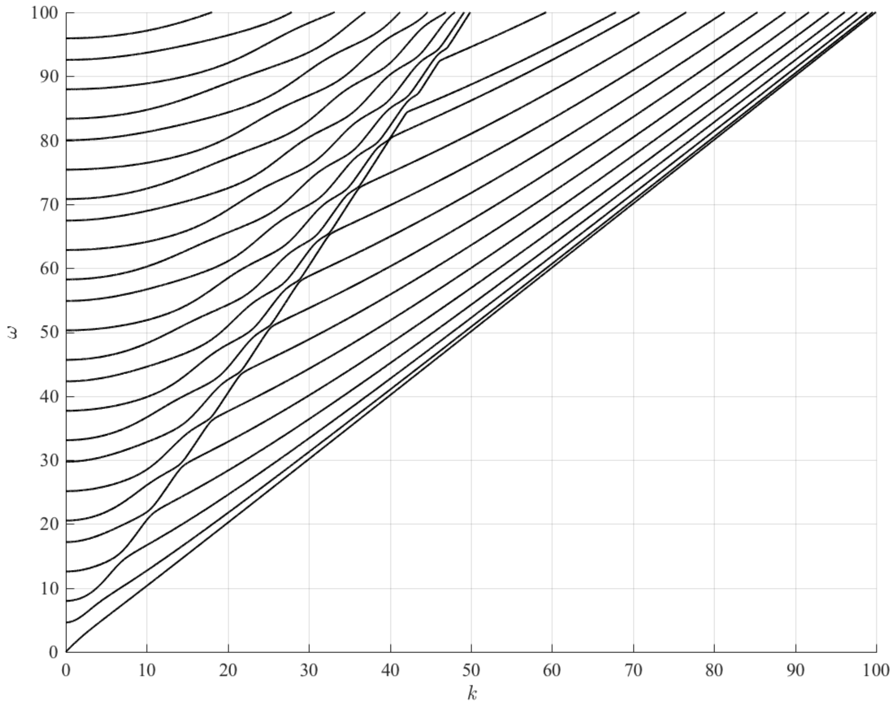

FIG. 10. *Dispersion relation of ω against k for the bilayer problem from (67) with $c_1 = 1$, $c_2 = 2$.*

Then, applying the calculus of residues, we see that the integrand has poles at $\omega = 0$ and $\pm\Omega_n (n = 0, 1, 2, ...)$ as defined in (71). Interestingly, the contributions from the poles at $\omega = \pm c_1 k$ in the second term of (66) cancel out those from the poles in the first term. Thus

$$\phi = 1 + \frac{4i}{\pi}\int_0^\infty \sin kX \left(\sum_{n=0}^{\infty} P_n(k)\cos\lambda_{1n}Y + Q_n(k)\sin\lambda_{1n}Y \right) \cos\Omega_n T dk \tag{74}$$

where

$$\lambda_{1n}{}^2 = \frac{\Omega_n{}^2}{c_1^2} - k^2, \tag{75}$$

and $P_n(k)$ and $Q_n(k)$ are the residues of P and Q at $\omega = \Omega_n$. A similar result holds for $0 < Y < 1/2$. We note that λ_{2n} is imaginary when $c_1 k < \Omega_n < c_2 k$, but that λ_{1n} is always real.

4.4. Large-time asymptotics. The first term in (74) is the steady state solution and the rest of the cumbersome expression in (74) is only useful in practice when we are considering the limit $X, T \to \infty$. With $X/T = O(1)$ we can then use the method of stationary phase to determine the leading-order terms. An observer moving with speed $V = X/T$ will see a complicated combination of leading-order waves which decay with amplitude $O(T^{-1/2})$ and travel with the group velocity $V = d\Omega_n/dk$. However, if V is such that $d^2\Omega_n/dk^2 = 0$, the amplitude of these waves will be enhanced.

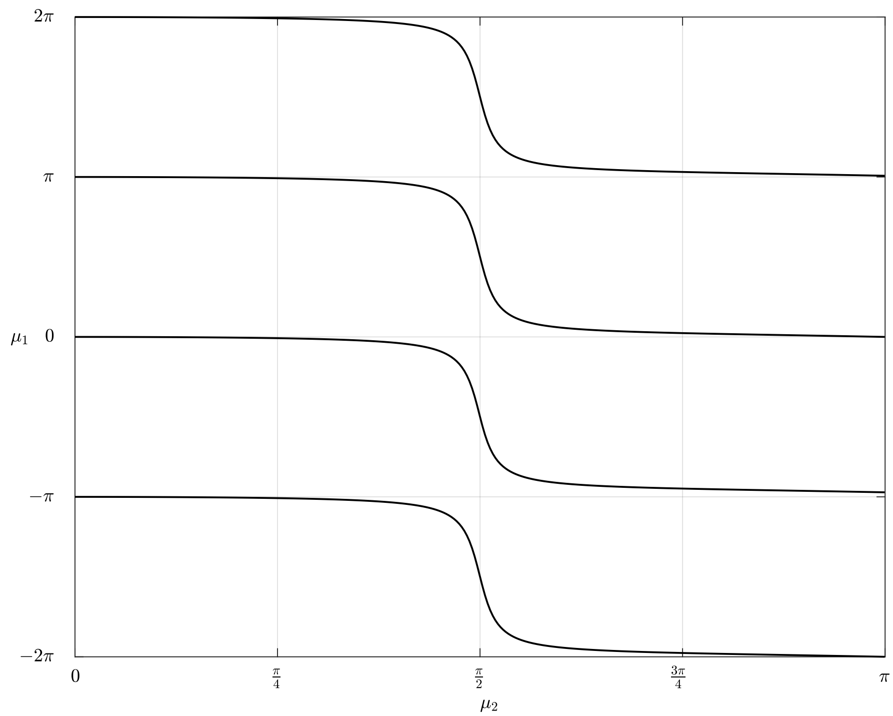

FIG. 11. *Curves in the μ_2, μ_1 plane given by zeros of the left-hand side of (72) when $n = 10$ and μ_2 is real.*

From Figure 10, we see that such inflection points in the dispersion relation occur at the origin, where $\omega = \Omega_0$, and that the number of points of inflection on $\omega = \Omega_n$ increases with n. As shown in [7], the contribution to ϕ from the neighbourhood of each inflection point is simply proportional to an Airy function of the first kind whose argument is proportional to $(X - c_H T)/T^{1/3}$. It thus represents a wave packet of width $O(T^{1/3})$ and amplitude $O(T^{-1/3})$. All these waves are, however, dwarfed by the contribution from the inflection point at the origin of the (ω, k) plane where the local dispersion relation is

$$\omega^2(k) = c_H^2 k^2 - \frac{(c_2^2 - c_1^2)^2}{(c_2^2 + c_1^2)^2}\frac{k^4}{12} + O(k^6), \tag{76}$$

which is in accordance with (34) of [8].

The new feature is that the stationary phase contribution from $k = 0$ is amplified by the presence of a pole in the first term of (74). Using the same stationary phase method that was described in [7] to evaluate the contour integral in (74), the dominant contribution to ϕ is the integral of an Airy Function whose argument is proportional to $(X - c_H T)T^{-1/3}$ and is given by

$$\frac{\partial \phi}{\partial \zeta} \sim (\text{const.})\Big(\frac{2}{T\omega'''(0)}\Big)^{1/3}\mathrm{Ai}\bigg(\Big(\frac{2}{-T\omega'''(0)}\Big)^{1/3}(X - c_H T)\bigg), \tag{77}$$

where $\zeta = X - c_H T$. From (76), $\omega'''(0)$ is negative and hence ϕ consists of a smooth jump, which does not decay in time, followed by a decaying dispersive wavetrain. This is consistent with solutions of the homogeneous equation (7) and also the numerical solution in Figures 6 and 7.

In summary, this analysis not only corroborates the homogenisation theory of section 1 but also reveals further interesting features. In particular for ω, k of $O(1)$ it indicates the presence of trains of wave packets corresponding to the stationary phase contributions from the inflection points in Figure 10 which propagate behind the dominant wave (77) in both layers. In particular, for ω, k large, the geometry of the curves in Figure 10 shows how these contributions combine on $\omega = c_2 k$ to create a spike at $X = c_2 T$. Also from Figure 10 it can be seen that the series (74) has singular behaviour near the branch $\omega = c_1 k$ which is due to the unit jump in this layer at $X = c_1 T$ which continues to propagate with speed c_1 even though the wave form decays rapidly immediately behind the jump. This thus generates a spike that gets thinner as T increases.

5. Conclusion. Possibly the most surprising result to emerge from this investigation is the close similarity between the detailed waveform in the far field for waves propagating parallel and perpendicular to the strata in a periodically layered medium. Not only is the speed c_H of the dominant wave the same in either case, but the waveform adopted by an initial step-function pulse is always the integral of an Airy function in a frame moving with c_H.

There are marked differences between the exact and homogenised solutions when we compare parallel and transverse propagation. In both cases the long-time solution contains bursts of localised waves that spread out behind the leading homogenised wavefront, but, in the parallel case, we also see localised decaying pulses travelling with the wave speed in each layer; however, as shown in [7], for the transverse case the leading disturbance travels at a speed $\left[\overline{\dfrac{1}{c}}\right]^{-1}$, and its amplitude appears to decay exponentially with time. The behaviour of the pulses for the oblique case remains an open question.

A new phenomenon in the parallel case concerns the large-time limit of the local wave forms in the wavefront regions $X = c_i T$. These waveforms always contain a jump of unity at the wavefront. In the fast layer, there is no precursor ahead of the front $X = c_2 T$ where $\phi = 1$, but the region behind this front becomes increasingly narrow and is followed by an oscillatory region where the amplitude is exponentially small as $T \to \infty$. In the slow layer, there are oscillations both ahead of and behind the jump at $X = c_1 T$, and the wavefield tends to unity as $(c_1 T - X)$ increases.

We also remark that our numerical and asymptotic analyses have been accurate enough to reveal that the only regions in which ϕ exhibits rapid change of $O(1)$ as $T \to \infty$ are the spikes near $X = c_i T$ and the jump near $X = c_H T$. We conjecture that these near singularities in the waveform tend to what is called a wave front set in the limit as $T \to \infty$ [1].

On the basis of the numerical evidence in [8], we confidently expect that a similar scenario will apply to general two-dimensional wave propagation in a layered medium.

Appendix. The expressions for P, Q, R and S in (66) are as follows:

$$
\begin{aligned}
P &= \frac{-ik\omega(c_2^2 - c_1^2)\tan\frac{\lambda_2}{2}}{c_1^2 c_2^2 \lambda_1^2 \lambda_2 \Delta} \\
Q &= \frac{ik\omega(c_2^2 - c_1^2)\tan\frac{\lambda_2}{2}\tan\frac{\lambda_1}{2}}{c_1^2 c_2^2 \lambda_1^2 \lambda_2 \Delta} \\
R &= \frac{ik\omega(c_2^2 - c_1^2)\tan\frac{\lambda_1}{2}}{c_1^2 c_2^2 \lambda_1 \lambda_2^2 \Delta} \\
S &= \frac{ik\omega(c_2^2 - c_1^2)\tan\frac{\lambda_1}{2}\tan\frac{\lambda_2}{2}}{c_1^2 c_2^2 \lambda_1 \lambda_2^2 \Delta}
\end{aligned}
\tag{78}
$$

where

$$\lambda_1^2 = \frac{\omega^2}{c_1^2} - k^2,\ \lambda_2^2 = \frac{\omega^2}{c_2^2} - k^2,$$

and

$$\Delta = \lambda_1 \tan\frac{\lambda_1}{2} + \lambda_2 \tan\frac{\lambda_2}{2}.$$

Acknowledgments. We wish to thank G. Benham (University of Oxford) for Figures 10 and 11. We also thank a referee for helpful remarks concerning anisotropy.

REFERENCES

[1] D. E. Edmunds, L. E. Fraenkel, and M. Pemberton, *Frederick Gerard Friedlander. 25 December 1917 – 20 May 2001*, Biogr. Mems Fell. R. Soc., 63 (2017), pp. 273 – 307.

[2] A. Erdélyi, ed., *Tables of Integral Transforms, Volume I*, McGraw-Hill Book Company, 1954.

[3] A. Erdélyi, ed., *Tables of Integral Transforms, Volume II*, McGraw-Hill Book Company, 1954.

[4] P. Goupillaud, *An approach to inverse filtering of near-surface layer effects from seismic records*, Geophysics, 36 (1961), pp. 754 – 760.

[5] J. Keller and A. Blank, *Diffraction and reflection of pulses by wedges and corners*, Communications in Pure and Applied mathematics, 4 (1951), pp. 75–95.

[6] R. LeVeque, *Finite Volume Methods for Hyperbolic Problems*, Cambridge University Press, 2002.

[7] H. Ockendon, J. R. Ockendon, C. L. Farmer, and D. J. Allwright, *One-dimensional wave dispersion in layered media*, SIAM J. Appl. Math, 75 (2015), p. 21282146, https://doi.org/10.1137/15M101138X.

[8] M. Quezada de Luna and D. Ketcheson, *Two-dimensional wave propagation in layered periodic media*, SIAM J. Appl. Math, 74 (2014), pp. 1852–1869, https://doi.org/10.1137/130937962.

[9] A. Shanin, *Precursor wave in a layered waveguide*, J. Acoust. Soc. Am., 141 (2017), pp. 346–356, https://doi.org/10.1121/1.4973958.

[10] G. Strang, *Accurate partial difference methods I: Linear Cauchy problems*, Arch. Rational Mech. Anal., 12 (1963), pp. 392 – 402.